GEOLOGY | THE GEOLOGICAL SOCIETY OF AMERICA®

https://doi.org/10.1130/G49633.1

Manuscript received 21 April 2021
Revised manuscript received 26 August 2021
Manuscript accepted 3 February 2022

Published online 14 April 2022

© 2022 Geological Society of America. For permission to copy, contact editing@geosociety.org.

Seismic anisotropy in the central Tien Shan unveils rheology-controlled deformation during intracontinental orogenesis

Bingfeng Zhang, Xuewei Bao* and Yixian Xu
Key Laboratory of Geoscience Big Data and Deep Resource of Zhejiang Province, School of Earth Sciences, Zhejiang University, Hangzhou 310027, China

ABSTRACT

The initiation and evolution of compressional intracontinental orogens are favored by rheologically weak lithosphere underneath; however, how this weakened lithosphere responds to the regional stress regime remains vigorously debated. The Tien Shan mountains in central Asia provide the best example to illustrate the deep deformational responses to intracontinental orogenesis. We present new constraints on the nature of seismic anisotropy in the crust and upper mantle of the central Tien Shan through shear-wave splitting analyses. Our results reveal a sharp change in the orientations of crustal anisotropic fabrics on two sides of the mountains. The convergence-parallel fast orientations in the northern segment are closely related to the lower-crustal simple-shear deformation caused by the underthrusting of the Kazakh Shield, whereas the depth-independent orogen-parallel fast orientations in the southern segment suggest vertically coherent pure-shear thickening of the Tien Shan lithosphere in response to the northward indentation of the Tarim Basin. The thickened lithosphere has partly foundered into the deep mantle, contributing to the accelerated shortening deformation in the late Cenozoic. Our observations demonstrate the complex tectonic processes in the Tien Shan and suggest that the rheological properties of bounding blocks can play a significant role in shaping the lithospheric structures of intracontinental orogens.

INTRODUCTION

Intracontinental orogens are highly uplifted regions that develop away from plate boundaries due to transmitted compressional stress from plate-margin interactions. The ongoing intense tectonic activity in the Tien Shan (central Asia), situated ~2000 km north of the Indo-Eurasian collision zone (Fig. 1), offers an excellent opportunity for investigating the modes of strain accommodation during intracontinental orogenesis. Important clues have been provided by seismic imaging of the crust and mantle; however, the interpretation of the revealed deep structures remains inconclusive. For example, the observations of high-velocity anomalies in the upper mantle and thickened mantle transition zone have been attributed to either (1) the underthrusting of the Kazakh Shield and Tarim Basin lithospheres followed by breakoff of the downgoing slabs, or (2) convective thinning of the thickened Tien Shan lithosphere itself due to gravitational instability (Lei and Zhao, 2007; Li et al., 2009; Tian et al., 2010). Moreover, the notion of two-sided underthrusting has recently been challenged by two receiver function (RF) studies in the central and eastern Tien Shan (Li et al., 2016; Zhang et al., 2020), where the Moho topography suggests only the southward underthrusting of the Kazakh Shield and the Junggar Basin beneath the belt. A recent high-resolution continent-scale lithospheric S-wave velocity (Vs) model (Bao et al., 2015) also shows limited evidence for northward and southward underthrusting of the Tarim Basin beneath the Tien Shan and the Tibetan Plateau, respectively.

Seismic anisotropy provides critical constraints on deformation mechanisms at depth. The lattice preferred orientation (LPO) of anisotropic minerals in mantle peridotite tends to run parallel to the strike of the Tien Shan; however, the cause of such parallelism is still under debate (Makeyeva et al., 1992; Li and Chen, 2006; Li et al., 2010). Several hypotheses have been proposed, including coherent lithospheric shortening in response to north-south compression, orogen-parallel mantle flow, and absolute plate motion (APM)–induced LPO in the asthenosphere. Currently, however, constraints on crustal anisotropy are limited by few studies with insufficient lateral resolution (Vinnik et al., 2007; Guo et al., 2017), although crustal deformation is more directly linked to the Cenozoic orogenesis. We present new information about the across-strike variations of anisotropic structures within the crust and upper mantle of the central Tien Shan, which illuminate lithospheric deformation processes in unprecedented detail. The revealed contrasting deformation on the two sides of the Tien Shan may offer fresh insights into the long-lasting question about the deformation mechanisms of intracontinental orogens.

LATERAL VARIATIONS IN SHEAR-WAVE SPLITTING OBSERVATIONS

Data used in this study are mainly from the passive seismic experiment of the Middle Asian Active Source (MANAS) project, supplemented by seismograms from several Kyrgyz Seismic Telemetry Network (KNET), Kyrgyz Digital Network (KRNET), and Tien Shan Continental Dynamic project (GHENGIS) stations (Table S3 in the Supplemental Material[1]). The 55 broadband seismograph stations constitute a NNW-SSE–trending profile across the central Tien Shan with an interstation spacing of ~10 km, providing an excellent opportunity for probing

*E-mail: xwbao@zju.edu.cn

[1]Supplemental Material. Detailed descriptions of the data, methods, and quality assessment specifics, discussion on the azimuthal variations of the XKS splitting measurements, and supplemental Figures S1–S7 and Tables S1–S6. Please visit https://doi.org/10.1130/GEOL.S.19424348 to access the supplemental material, and contact editing@geosociety.org with any questions.

CITATION: Zhang, B., Bao, X., and Xu, Y., 2022, Seismic anisotropy in the central Tien Shan unveils rheology-controlled deformation during intracontinental orogenesis: Geology, v. XX, p. , https://doi.org/10.1130/G49633.1

Downloaded from http://pubs.geoscienceworld.org/gsa/geology/article-pdf/doi/10.1130/G49633.1/5586017/g49633.pdf
by Zhejiang University user

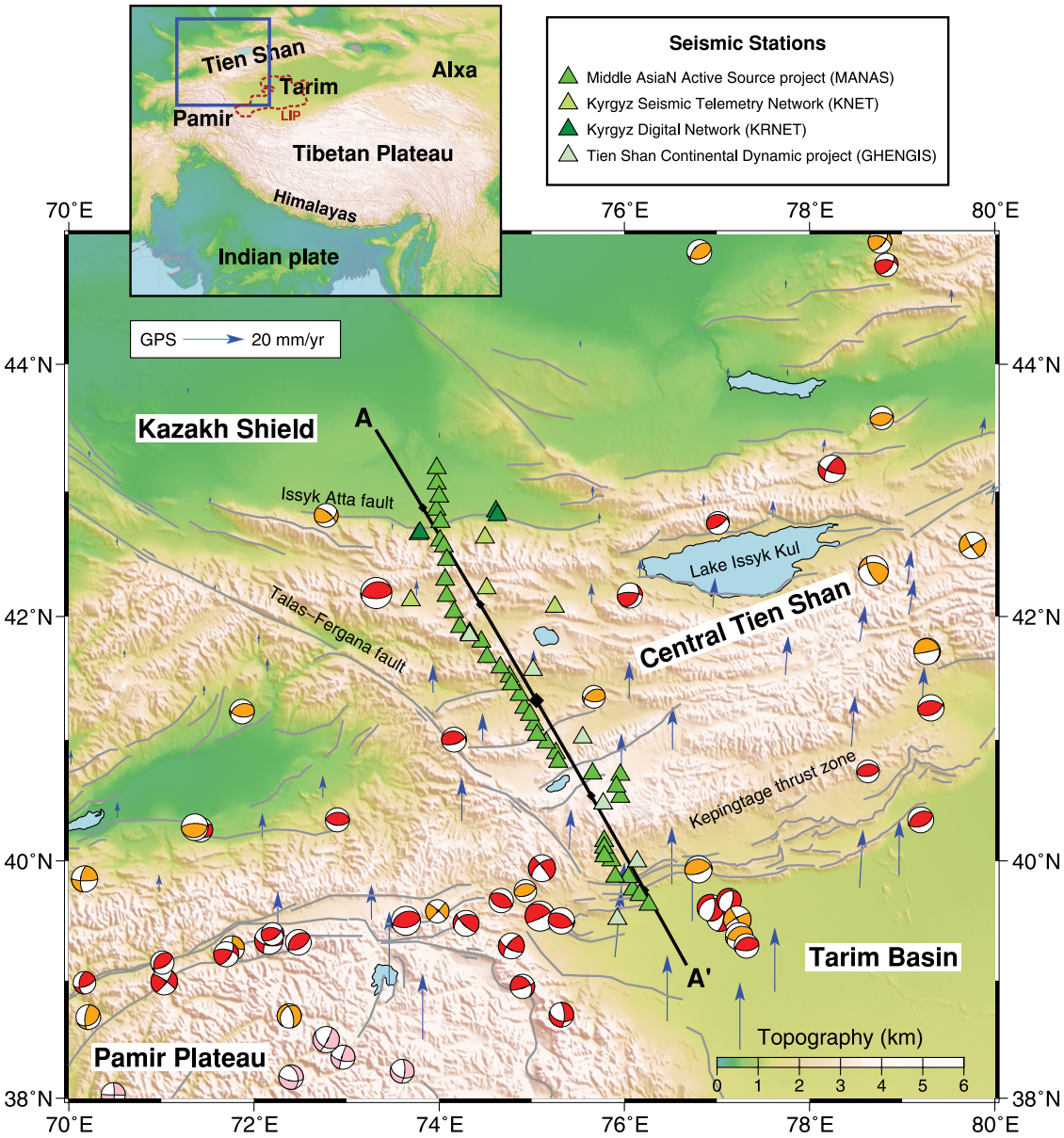

Figure 1. Shaded-relief map of the central Tien Shan (central Asia) and surrounding areas. Gray thin lines show major fault traces from Styron and Pagani (2020). Stations from different data sources are marked as triangles. Location of the study area (blue box) and the Tarim large igneous province (LIP) are indicated in top left inset. Blue arrows denote GPS velocities relative to Eurasia (Zubovich et al., 2010). Beach balls show focal mechanisms (Ekström et al., 2012) for large earthquakes (M_b >5.5) since 1976 CE where event depths are indicated by different colors (red: 0–20 km, orange: 20–50 km, and pink: 50–150 km). Relief data are from the SRTM30 digital elevation model (https://topex.ucsd.edu/WWW_html/srtm30_plus.html). Line A-A′ shows the projected profile in Figure 3. The origin, ±100 km, and ±200 km nodes on the profile are also marked for clarity.

fine structures of the crust and upper mantle in the region (Fig. 1).

Shear-wave splitting (SWS) observations of fast orientation (ϕ) and delay time (δt) offer direct diagnostics of deformation-related anisotropic structures at depth. Here, SWS analyses are performed on Moho P-to-S (Ps) converted waves on RFs (Pms waves) and on core-refracted SKS/SKKS waves (XKS waves) to constrain crustal anisotropy and apparent anisotropy of crust and upper mantle, respectively. The former procedure is based on the least-squares harmonic fitting of Pms arrival times at different back azimuth (Liu and Niu, 2012), while the latter is carried out in SplitRacer code using the minimum energy method (Reiss and Rümpker, 2017).

We report 27 well-constrained crustal anisotropy measurements and 435 new XKS splitting observations at 40 MANAS stations (Fig. 2; Fig. S1 and Tables S1 and S2). No explicit spatial variation of the ϕ_{XKS} measurements was observed. The fast orientations agree well with previous results (Makeyeva et al., 1992; Li and Chen, 2006) and generally fluctuate around 64°, roughly parallel to the mountain strike. The average δt_{XKS} over all measurements is 1.06 ± 0.25 s. We also noticed some azimuthal variation in the XKS measurements (Fig. S2), which is likely associated with the localized strong anisotropy in the deep mantle (see details in the Supplemental Material). In contrast, Pms moveout fitting measurements vary significantly along the profile. A sharp contrast of ϕ_{Pms} is revealed between the north-central and south-central Tien Shan (NCTS and SCTS, respectively), with mostly north-south or northwest-southeast (convergence-parallel) measurements for the northern part and ENE-WSW (orogen-parallel) for the southern part. The outliers may be related to nearby fault-zone fabrics (for stations near the Issyk Atta fault and southernmost segment of the Talas-Fergana fault) or fossil anisotropic structures retained in the crust (for stations in the Naryn Basin). The average δt_{Pms} of 0.60 s emphasizes the contribution of crustal deformation to the observed XKS splitting.

DISCUSSION

Underthrusting of the Kazakh Shield beneath the NCTS

There are different origins for convergence-parallel anisotropy at different depths. In the continental upper crust, stress-aligned fluid-saturated cracks generally produce azimuthal anisotropy with $\delta t < 0.2$ s (Crampin, 1994), inconsistent with the large splitting in the NCTS, hinting at a deeper origin of the observed anisotropy. Due to the closure of cracks, the LPO of

Downloaded from http://pubs.geoscienceworld.org/gsa/geology/article-pdf/doi/10.1130/G49633.1/5586017/g49633.pdf
by Zhejiang University user

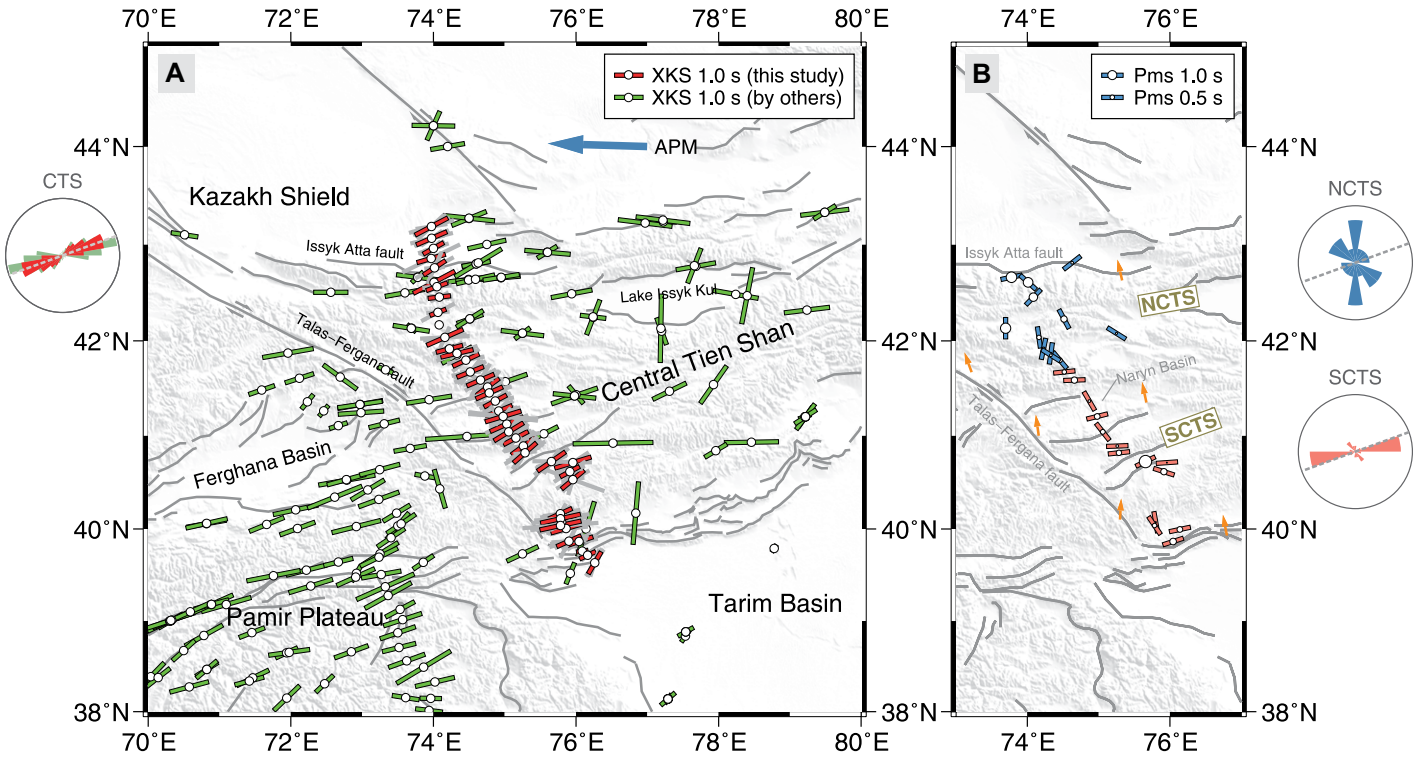

Figure 2. Map view of seismic anisotropy measurements. (A) Station-averaged XKS splitting measurements obtained in this study (red bars) and previous studies (green bars; Wüstefeld et al., 2009). Individual measurements from this study are also indicated by gray bars. Fast axis and amount of splitting are shown by orientation and length of bar line, respectively. Blue arrow denotes the absolute plate motion (APM) direction of the Eurasian plate in a hotspot frame (HS3-NUVEL1A). Rose diagram to the left demonstrates good correspondence between fast orientations from this (red) and previous (green) studies, as well as the strike (dashed line) of the central Tien Shan (CTS). (B) Crustal anisotropy parameters measured from the Moho P-to-S converted waves on receiver functions (Pms waves). Fast axis and amount of splitting are shown by the orientation of the bar line and size of the circle, respectively. Orange arrows show maximum horizontal compressional stress direction (Heidbach et al., 2018). Rose diagrams to the right denote distribution of fast orientations for the north-central Tien Shan (NCTS) and south-central Tien Shan (SCTS) measurements.

anisotropic minerals, in particular amphibole, is the primary cause for anisotropic fabrics in the deep crust. Ko and Jung (2015) found that simple-shear deformation of amphibole produces enhanced LPO structures with shear-parallel fast orientation in a high-temperature environment. The development of such foliation planes has been observed in compressional orogens worldwide as an indicator of plate subduction beneath (Huang et al., 2015). The coherence between ϕ_{Pms} and the dip direction of the Kazakh Shield (Zhang et al., 2020) thus suggests that the observed crustal anisotropy largely results from simple shear between the southward-underthrusting Kazakh lower crust and the overlying Tien Shan crust. This inference is consistent with the imaged southward-dipping high-velocity anomaly in the region, which corresponds to the underthrusted Kazakh lithosphere (Lei and Zhao, 2007).

Taking into consideration the similar LPO manners of amphibole and olivine (Zhang and Karato, 1995; Ko and Jung, 2015), orthogonal ϕ_{Pms} and ϕ_{XKS} measurements observed in the NCTS suggest contrasting deformation styles between the crust and upper mantle. Therefore, it would be expected that crustal anisotropy is manifested in the XKS splitting and/or compensated by the enhanced deformation in the upper mantle. Indeed, decreased δt_{XKS} is found where the strength of convergence-parallel crustal anisotropy reaches its maximum at ~130 km along the profile (Fig. 2; Fig. S1). The thickened mantle lithosphere in the NCTS (Kumar et al., 2005) could also accommodate more deformation that contributes to the XKS splitting as compared to the SCTS. Furthermore, we suggest that the fossil anisotropic fabrics within the underthrusted Kazakh mantle lithosphere might be responsible for the enhanced upper-mantle anisotropy in the NCTS, in view of the similarly oriented XKS measurements in the interior of the Kazakh Shield.

Vertically Coherent Deformation within the SCTS Lithosphere

Pn (P wave bottoming in the uppermost mantle) anisotropy tomography (Zhou and Lei, 2015) reveals significant azimuthal anisotropy with orogen-parallel (ENE-WSW) fast orientations in the uppermost mantle of the SCTS. Here, similarly oriented anisotropy is also derived from XKS splitting and Pms moveout fitting analyses for SCTS stations. This striking parallelism between fast orientations determined independently from three data sets with distinct depth sensitivity suggests that the SCTS may be characterized by a single layer of anisotropy. This also argues for vertically coherent lithospheric shortening and thickening rather than orogen-parallel mantle flow as the source of anisotropy in the SCTS. The north-south compression induced by northward indentation of the Tarim Basin promotes the pure-shear deformation of anisotropic minerals and aligns them in the orogen-parallel direction. The crust and mantle are coupled and deform coherently, generating the observed ~4% seismic anisotropy throughout the lithosphere. The northward subduction of the Tarim Basin, however, is unlikely to have occurred in the SCTS, given that the observed orogen-parallel ϕ_{Pms} is incompatible with the predicted NNW-SSE alignment of minerals due to strong shear deformation along the subduction interface.

The Moho discontinuity is imaged at ~60 km depth beneath the SCTS (Zhang et al., 2020), which is the product of significant crustal thickening during Cenozoic orogenesis, considering the crustal thickness of 35–40 km at ca. 70 Ma (Bagdassarov et al., 2011). The strong coupling of the whole lithosphere as proposed above predicts similarly thickened lithospheric mantle to a depth of ~150 km, much deeper than the current

Downloaded from http://pubs.geoscienceworld.org/gsa/geology/article-pdf/doi/10.1130/G49633.1/5586017/g49633.pdf
by Zhejiang University user

seismological lithosphere-asthenosphere boundary (~100 km depth) there. Therefore, we suggest that the lower part of the thickened lithosphere in the Tarim–Tien Shan junction zone has foundered into the deep mantle by gravitational instability with the aid of edge-driven convection (Bao et al., 2014). This geodynamic scenario is also supported by the imaged high-velocity structure in the mantle, which likely represents the detached lithosphere (Li et al., 2009).

A Conceptual Model for the Cenozoic Deformation of the Tien Shan

Our observations provide new and direct evidence to support the one-sided underthrusting scenario and extend this view to the whole lithosphere, in which only the Kazakh Shield and Junggar Basin lithosphere to the north underthrust the Tien Shan whereas the Tarim Basin cratonic lithosphere to the south merely indents northward subhorizontally. We suggest that this across-strike varying deformation response of the Tien Shan can be primarily attributed to the contrasting rheology of the bounding tectonic blocks. Large lithospheric strength contrast with adjacent blocks (Deng et al., 2017) and preexisting faults inherited from Paleozoic accretion (Tapponnier and Molnar, 1976) are regarded as the fundamental causes for the strain concentration of the Tien Shan in response to the India-Eurasia collision. Rheological properties also vary between the bounding blocks to the north and the south of the orogen. For instance, the Junggar Basin is underlain by a trapped Paleozoic oceanic plate with relatively high density, high velocity, and low Mg# (Zhang et al., 2019). The high-velocity Tarim mantle lithosphere, on the other hand, is melt depleted, buoyant, and mechanically resistant in nature (Bao et al., 2015; Deng et al., 2017), typical of an Archean craton. These characteristics are further enhanced by Permian plume magmatism in the Tarim Basin (Y.G. Xu et al., 2014; X. Xu et al., 2020), which defines a large igneous province of more than 250,000 km^2. As a result, the buoyant and strengthened Tarim cratonic materials would be more resistant to subduction than the bounding blocks to the north and subhorizontally indent the Tien Shan instead. On the other hand, thermal state and compressional stress may not exert a primary control on the deformation patterns in an intracontinental setting, given that two-sided underthrusting is dominant in numerical simulations with the same lithospheric strength for the Tarim and Junggar Basins and varying geotherms and convergence rates for the Tien Shan (Huangfu et al., 2021).

Based on our results and previous observations, we propose a new tectonic model for the Cenozoic intracontinental orogenesis of the Tien Shan (Fig. 3). Prior to the significant uplifting since 20–25 Ma, the Tien Shan was a peneplain, resulting from the long-term denudation and planation of both surface and lithospheric structures. Then, as enhanced stress by the India-Eurasia collision was transferred into the interior of Eurasia, rheology-controlled intraplate strain concentration resumed tectonic activity in the Tien Shan. Because of the contrasting lithospheric rheology between the northern and southern bounding blocks, the deformation response on the two sides of the orogen was dramatically different. The Kazakh Shield and Junggar Basin lithosphere to the north underthrusted the northern part of the Tien Shan at 8–10 mm

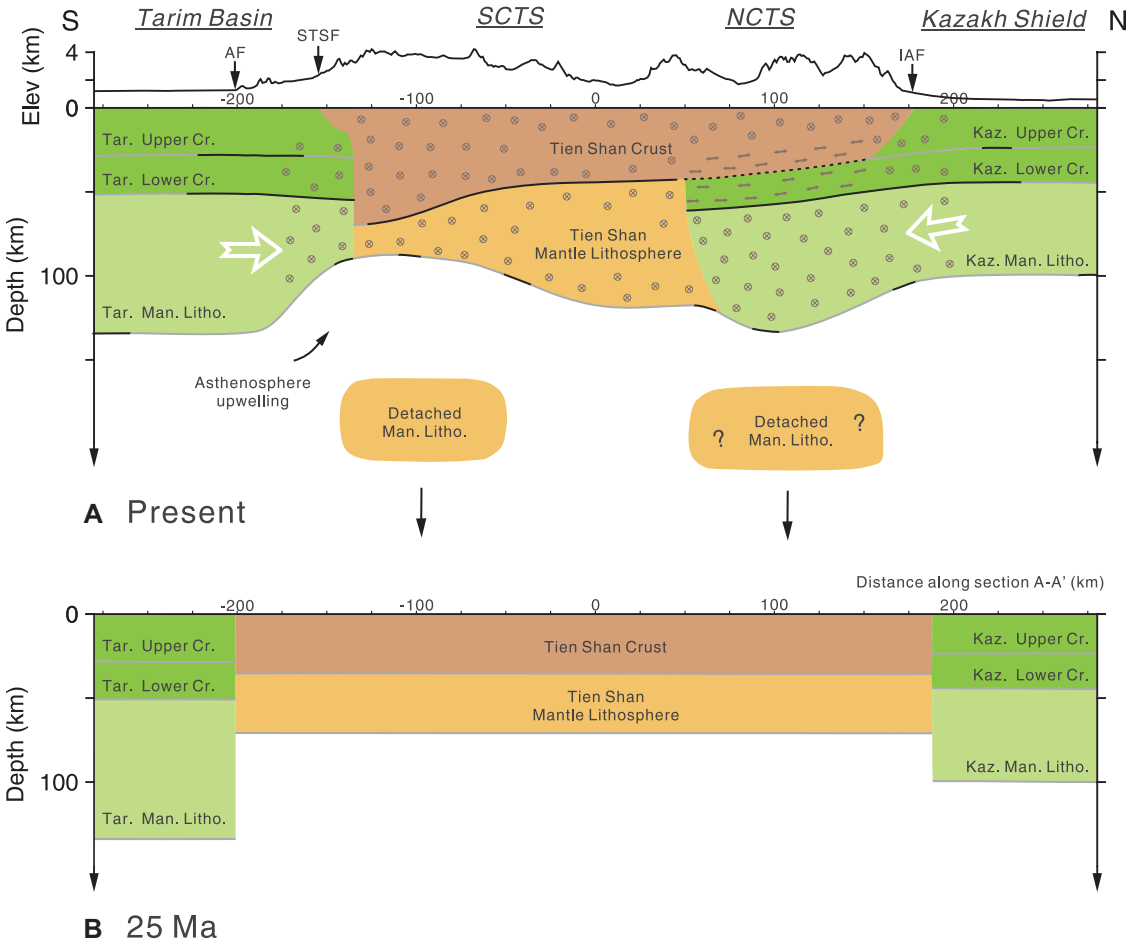

Figure 3. Schematic illustration of lithospheric structures and associated deformation processes beneath the Tien Shan (central Asia) along profile A-A′ in Figure 1. (A) At present, the lower part of the Kazakh Shield lithosphere underthrusts the northern Tien Shan, whereas indentation of the Tarim Basin lithosphere to the south resulted in coherent shortening and thickening of the lithosphere, which was followed by foundering of the lithospheric root. Characteristic fast orientations are shown on both sides of the orogen (double-arrow symbols: convergence-parallel anisotropy; circled-X symbols: orogen-parallel anisotropy). Moho and lithosphere-asthenosphere boundary topography are constrained by two receiver function studies (Kumar et al., 2005; Zhang et al., 2020), as shown in black thick lines. Detached Tien Shan mantle lithospheres are inferred from a regional tomographic model (Li et al., 2009). (B) Initial state of the Tien Shan lithosphere prior to Cenozoic orogenesis (ca. 25 Ma). Note the flattened subsurface interfaces and significantly thinned crust (35–40 km) and lithosphere (~70 km) (Bagdassarov et al., 2011) as a result of long-term planation in the Mesozoic. Elevation along profile A-A′ is also shown on the top. Elev—elevation; AF—Atushi fault; STSF—South Tien Shan fault; SCTS—south-central Tien Shan; NCTS—north-central Tien Shan; IAF—Issyk Atta fault; Tar.—Tarim; Kaz.—Kazakh; Cr.—crust; Man. Lithos.—mantle lithosphere.

Downloaded from http://pubs.geoscienceworld.org/gsa/geology/article-pdf/doi/10.1130/G49633.1/5586017/g49633.pdf
by Zhejiang University user

yr^{-1}, given the Moho overlap of 90–110 km (Li et al., 2016; Zhang et al., 2020) and the initiation of deformation at ca. 11 Ma there (Bullen et al., 2003). In the southern part of the central Tien Shan, the buoyant and strengthened Tarim Basin lithosphere indented rather than subducted under the mountains, resulting in the vertically coherent thickening and subsequent foundering of the Tien Shan lithosphere. Numerical modeling has shown that when convergence rate is high, which is the case for the central Tien Shan, there is accelerated contraction and thickening rather than extension of the crust in response to lithospheric foundering (Göğüş and Pysklywec, 2008). Thus, the subsequent foundering of ~50-km-thick lithospheric root may be responsible for the accelerated shortening deformation of the central Tien Shan in the late Cenozoic (Heermance et al., 2008).

CONCLUSIONS

The new constraints on across-strike variations of seismic anisotropy presented here reveal distinct deformation responses in the northern and southern parts of the Tien Shan, which are closely related to the rheologic properties of neighboring terranes. This finding highlights the important contribution of lithospheric rheology to not only the strain localization during intracontinental orogenesis but also the pattern of dynamic processes at depth.

ACKNOWLEDGMENTS

Seismic data are provided by the Incorporated Research Institutions for Seismology (IRIS) Data Management Center. Constructive comments from editor Chris Clark and five anonymous reviewers significantly improved the manuscript. This study is supported by the National Natural Science Foundation of China (grants 41774045 and 41830212).

REFERENCES CITED

Bagdassarov, N., Batalev, V., and Egorova, V., 2011, State of lithosphere beneath Tien Shan from petrology and electrical conductivity of xenoliths: Journal of Geophysical Research, v. 116, B01202, https://doi.org/10.1029/2009JB007125.

Bao, X.W., Eaton, D.W., and Guest, B., 2014, Plateau uplift in western Canada caused by lithospheric delamination along a craton edge: Nature Geoscience, v. 7, p. 830–833, https://doi.org/10.1038/ngeo2270.

Bao, X.W., Song, X.D., and Li, J.T., 2015, High-resolution lithospheric structure beneath Mainland China from ambient noise and earthquake surface-wave tomography: Earth and Planetary Science Letters, v. 417, p. 132–141, https://doi.org/10.1016/j.epsl.2015.02.024.

Bullen, M.E., Burbank, D.W., and Garver, J.I., 2003, Building the northern Tien Shan: Integrated thermal, structural, and topographic constraints: The Journal of Geology, v. 111, p. 149–165, https://doi.org/10.1086/345840.

Crampin, S., 1994, The fracture criticality of crustal rocks: Geophysical Journal International, v. 118, p. 428–438, https://doi.org/10.1111/j.1365-246X.1994.tb03974.x.

Deng, Y.F., Levandowski, W., and Kusky, T., 2017, Lithospheric density structure beneath the Tarim basin and surroundings, northwestern China, from the joint inversion of gravity and topography: Earth and Planetary Science Letters, v. 460, p. 244–254, https://doi.org/10.1016/j.epsl.2016.10.051.

Ekström, G., Nettles, M., and Dziewoński, A.M., 2012, The global CMT project 2004–2010: Centroid-moment tensors for 13,017 earthquakes: Physics of the Earth and Planetary Interiors, v. 200–201, p. 1–9, https://doi.org/10.1016/j.pepi.2012.04.002.

Göğüş, O.H., and Pysklywec, R.N., 2008, Mantle lithosphere delamination driving plateau uplift and synconvergent extension in eastern Anatolia: Geology, v. 36, p. 723–726, https://doi.org/10.1130/G24982A.1.

Guo, Z., Gao, X., Yao, H.J., and Wang, W., 2017, Depth variations of azimuthal anisotropy beneath the Tian Shan Mt range (NW China) from ambient noise tomography: Journal of Asian Earth Sciences, v. 138, p. 161–172, https://doi.org/10.1016/j.jseaes.2016.12.040.

Heermance, R.V., Chen, J., Burbank, D.W., and Miao, J.J., 2008, Temporal constraints and pulsed Late Cenozoic deformation during the structural disruption of the active Kashi foreland, northwest China: Tectonics, v. 27, TC6012, https://doi.org/10.1029/2007TC002226.

Heidbach, O., et al., 2018, The World Stress Map database release 2016: Crustal stress pattern across scales: Tectonophysics, v. 744, p. 484–498, https://doi.org/10.1016/j.tecto.2018.07.007.

Huang, T.Y., Gung, Y., Kuo, B.Y., Chiao, L.Y., and Chen, Y.N., 2015, Layered deformation in the Taiwan orogen: Science, v. 349, p. 720–723, https://doi.org/10.1126/science.aab1879.

Huangfu, P.P., Li, Z.H., Zhang, K.J., Fan, W.M., Zhao, J.M., and Shi, Y.L., 2021, India-Tarim lithospheric mantle collision beneath western Tibet controls the Cenozoic building of Tian Shan: Geophysical Research Letters, v. 48, e2021GL094561, https://doi.org/10.1029/2021GL094561.

Ko, B., and Jung, H., 2015, Crystal preferred orientation of an amphibole experimentally deformed by simple shear: Nature Communications, v. 6, https://doi.org/10.1038/ncomms7586.

Kumar, P., Yuan, X., Kind, R., and Kosarev, G., 2005, The lithosphere-asthenosphere boundary in the Tien Shan–Karakoram region from S receiver functions: Evidence for continental subduction: Geophysical Research Letters, v. 32, L07305, https://doi.org/10.1029/2004GL022291.

Lei, J.S., and Zhao, D.P., 2007, Teleseismic P-wave tomography and the upper mantle structure of the central Tien Shan orogenic belt: Physics of the Earth and Planetary Interiors, v. 162, p. 165–185, https://doi.org/10.1016/j.pepi.2007.04.010.

Li, A.B., and Chen, C.Z., 2006, Shear wave splitting beneath the central Tien Shan and tectonic implications: Geophysical Research Letters, v. 33, L22303, https://doi.org/10.1029/2006GL027717.

Li, J.Y., et al., 2016, Mantle subduction and uplift of intracontinental mountains: A case study from the Chinese Tianshan Mountains within Eurasia: Scientific Reports, v. 6, 28831, https://doi.org/10.1038/srep28831.

Li, Y.H., Wu, Q.J., Jiang, L.J., and Zhang, R.Q., 2010, Complex seismic anisotropic structure beneath the central Tien Shan revealed by shear wave splitting analyses: Geophysical Journal International, v. 181, p. 1678–1686, https://doi.org/10.1111/j.1365-246X.2010.04589.x.

Li, Z.W., Roecker, S., Li, Z.H., Wei, B., Wang, H.T., Schelochkov, G., and Bragin, V., 2009, Tomographic image of the crust and upper mantle beneath the western Tien Shan from the MANAS broadband deployment: Possible evidence for lithospheric delamination: Tectonophysics, v. 477, p. 49–57, https://doi.org/10.1016/j.tecto.2009.05.007.

Liu, H.F., and Niu, F.L., 2012, Estimating crustal seismic anisotropy with a joint analysis of radial and transverse receiver function data: Geophysical Journal International, v. 188, p. 144–164, https://doi.org/10.1111/j.1365-246X.2011.05249.x.

Makeyeva, L.I., Vinnik, L.P., and Roecker, S.W., 1992, Shear-wave splitting and small-scale convection in the continental upper mantle: Nature, v. 358, p. 144–147, https://doi.org/10.1038/358144a0.

Reiss, M.C., and Rümpker, G., 2017, SplitRacer: MATLAB code and GUI for semiautomated analysis and interpretation of teleseismic shear-wave splitting: Seismological Research Letters, v. 88, p. 392–409, https://doi.org/10.1785/0220160191.

Styron, R., and Pagani, M., 2020, The GEM Global Active Faults Database: Earthquake Spectra, v. 36, no. 1, Suppl., p. 160–180, https://doi.org/10.1177/8755293020944182.

Tapponnier, P., and Molnar, P., 1976, Slip-line field theory and large-scale continental tectonics: Nature, v. 264, p. 319–324, https://doi.org/10.1038/264319a0.

Tian, X.B., Zhao, D.P., Zhang, H.S., Tian, Y., and Zhang, Z.J., 2010, Mantle transition zone topography and structure beneath the central Tien Shan orogenic belt: Journal of Geophysical Research, v. 115, B10308, https://doi.org/10.1029/2008JB006229.

Vinnik, L.P., Aleshin, I.M., Kiselev, S.G., Kosarev, G.L., and Makeyeva, L.I., 2007, Depth localized azimuthal anisotropy from SKS and P receiver functions: The Tien Shan: Geophysical Journal International, v. 169, p. 1289–1299, https://doi.org/10.1111/j.1365-246X.2007.03394.x.

Wüstefeld, A., Bokelmann, G., Barruol, G., and Montagner, J.-P., 2009, Identifying global seismic anisotropy patterns by correlating shear-wave splitting and surface-wave data: Physics of the Earth and Planetary Interiors, v. 176, p. 198–212, https://doi.org/10.1016/j.pepi.2009.05.006.

Xu, X., Zuza, A.V., Yin, A., Lin, X.B., Chen, H.L., and Yang, S.F., 2020, Permian plume-strengthened Tarim lithosphere controls the Cenozoic deformation pattern of the Himalayan-Tibetan orogen: Geology, v. 49, p. 96–100, https://doi.org/10.1130/G47961.1.

Xu, Y.G., Wei, X., Luo, Z.Y., Liu, H.Q., and Cao, J., 2014, The Early Permian Tarim Large Igneous Province: Main characteristics and a plume incubation model: Lithos, v. 204, p. 20–35, https://doi.org/10.1016/j.lithos.2014.02.015.

Zhang, A.Q., Afonso, J.C., Xu, Y.X., Wu, S.C., Yang, Y.J., and Yang, B., 2019, The deep lithospheric structure of the Junggar Terrane, NW China: Implications for its origin and tectonic evolution: Journal of Geophysical Research: Solid Earth, v. 124, p. 11,615–11,638, https://doi.org/10.1029/2019JB018302.

Zhang, B.F., Bao, X.W., and Xu, Y.X., 2020, Distinct orogenic processes in the South- and North-Central Tien Shan from receiver functions: Geophysical Research Letters, v. 47, e2019GL086941, https://doi.org/10.1029/2019GL086941.

Zhang, S.Q., and Karato, S.-i., 1995, Lattice preferred orientation of olivine aggregates deformed in simple shear: Nature, v. 375, p. 774–777, https://doi.org/10.1038/375774a0.

Zhou, Z.G., and Lei, J.S., 2015, Pn anisotropic tomography under the entire Tienshan orogenic belt: Journal of Asian Earth Sciences, v. 111, p. 568–579, https://doi.org/10.1016/j.jseaes.2015.06.009.

Zubovich, A.V., et al., 2010, GPS velocity field for the Tien Shan and surrounding regions: Tectonics, v. 29, TC6014, https://doi.org/10.1029/2010TC002772.

Printed in USA

Downloaded from http://pubs.geoscienceworld.org/gsa/geology/article-pdf/doi/10.1130/G49633.1/5586017/g49633.pdf
by Zhejiang University user